

# Computational Characterization of Sulfur–Oxygen Three-Electron-Bonded Radicals in Methionine and Methionine-Containing Peptides: Important Intermediates in One-Electron Oxidation Processes

Dariusz Pogocki,<sup>\*,§,‡</sup> Katarzyna Serdiuk,<sup>#</sup> and Christian Schöneich<sup>\*,§</sup>

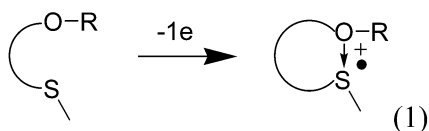
Department of Pharmaceutical Chemistry, University of Kansas, 2095 Constant Avenue, Lawrence, Kansas 66047, Institute of Chemistry, Pedagogical University, Armii Krajowej 13/15, 42-200 Częstochowa, Poland, and Institute of Nuclear Chemistry and Technology, Dorodna 16, 03-195 Warsaw, Poland

Received: March 28, 2003; In Final Form: June 9, 2003

Density functional theory and semiempirical methods were employed to characterize the structure and properties of sulfur–oxygen-bonded radical cations formed during the one-electron oxidation of various organic sulfides and methionine-containing peptides. In general, all of the examined sulfur–oxygen bonds can be described as two-center, three-electron-bonded systems. The usefulness of approximate computational approaches (SCC-DFTB, AM1 and PM3) for the reliable description of three-electron-bonded species was examined.

## Introduction

The nonbonded interaction between a divalent sulfur (S) and an oxygen (O) plays an important role for the structure and activity of organic sulfides and methionine-containing peptides.<sup>1–4</sup> Crystallographic and computational studies of native proteins have provided many examples for “nonbonded” sulfur–oxygen (S–O) interactions, predominantly for the 1,5-type but also for the 1,4- and 1,6-types.<sup>2</sup> Such S–O interactions could possibly modulate enzymatic activity<sup>5,6</sup> and control structures of folded proteins.<sup>7,8</sup> In addition, such a contingency may accelerate the one-electron (1e) oxidation of the divalent sulfur.<sup>9–13</sup> Usually, the 1e-oxidation of sulfides leads to sulfide radical cations which can subsequently complex, preferentially intramolecularly, with oxygen-carrying substituents such as hydroxy, alkoxy, or carboxylate groups (reaction 1).<sup>14–30</sup> The stabilization of the



1e-oxidized sulfur through formation of sulfur–oxygen bonded sulfuranyl radicals might potentially accelerate oxidation and autoxidation processes of substituted sulfides and of Met in peptides and proteins. For example, the electrochemical oxidation of dialkyl sulfides showed lower peak potentials when appended with neighboring carboxylate and alcohol groups.<sup>19,31–33</sup> Met oxidation is important during conditions of biological oxidative stress.<sup>9,34–37</sup> Specifically, the oxidation of Met<sup>35</sup> in  $\beta$ -amyloid peptides ( $\beta$ AP) 1–40 or 1–42, the major constituents of senile plaques in Alzheimer’s disease, has been associated with part of the neurotoxicity of these sequences.<sup>38,39</sup> In the helical C-terminus of  $\beta$ AP 1–40, the stabilization of oxidized

Met<sup>35</sup> through association with the C=O group of the peptide bond C-terminal to Ile<sup>31</sup> may be possible, as the ca. 3.6 Å average S–O distance between Met<sup>35</sup> and Ile<sup>31</sup>-C=O in the native sequence<sup>40</sup> is close to the sum of the van der Waals radii of the two atoms.<sup>41</sup> Our recent molecular modeling results<sup>42</sup> confirmed a “privileged” conformation of  $\beta$ -amyloid peptide congeners containing the  $\alpha$ -helical C-terminal sequence of  $\beta$ AP- (26–40) where structural and dynamic properties can promote the formation and stabilization of MetS<sup>•+</sup>. The tendency to stabilize MetS<sup>•+</sup> in the form of an S–O bond may explain the tendency of the native  $\beta$ AP1–40 to reduce Cu<sup>II</sup>,<sup>42,43</sup> generate free radicals, and induce protein oxidation. We have obtained direct experimental evidence for sulfide radical cation–amide association during the 1e-oxidation of Met in the model compound *N*-acetylmethionine amide<sup>44</sup> and in Met-containing model peptides,<sup>45</sup> supporting our hypothesis that such mechanisms may promote Met oxidation in  $\beta$ AP.

Unfortunately, the direct experimental detection of S–O-bonded intermediates in  $\beta$ AP by time-resolved spectroscopy is yet not possible due to the low solubility of these peptides. However, some structural and mechanistic details can be obtained through quantum chemical molecular modeling.

Therefore, in this paper we provide a detailed computational characterization of S–O-bonded radical structures of Met and Met-containing peptides. These results are directly applicable to redox processes of the macromolecule  $\beta$ AP. While ab initio calculations with large basis sets and including correlation are now approaching high accuracy, they are still limited to rather small systems. Semiempirical methods, on the other hand, are several orders of magnitude faster, thereby providing the possibility of gaining insight into the chemistry of larger systems. Unfortunately, most of the semiempirical methods today are based on the Hartree–Fock approximations AM1<sup>46,47</sup> and PM3,<sup>48,49</sup> which often fail in the accurate description of hypervalent compounds,<sup>50,51</sup> due to the employment of only a minimal sp-basis in the parametrization scheme. Specifically sulfur-containing molecules present a challenging task for approximate computational methods as calculations need to take into account the low-energy d-orbitals.<sup>51</sup> Nevertheless, we

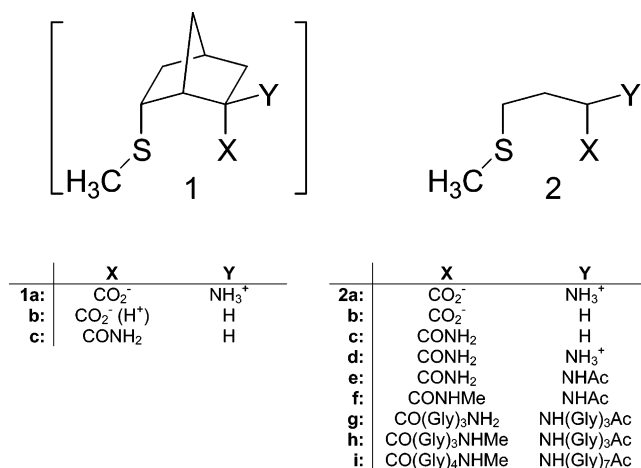
\* Address correspondence to this author. Fax: (785) 864-5736. E-mail: schoneic@ukans.edu.

§ University of Kansas.

‡ Institute of Nuclear Chemistry and Technology.

# Pedagogical University.

CHART 1



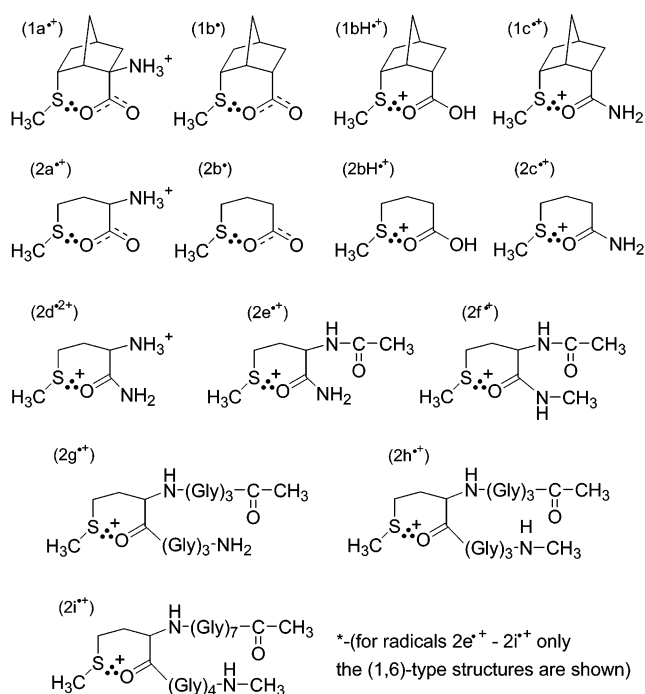
believe that there is need for a reliable semiempirical methodology to investigate the electronic structure of biological systems with sufficient accuracy and efficiency. Thus, part of this work focuses on the performance of a novel, approximate density-functional method (SCC-DFTB),<sup>51–59</sup> which runs 2–3 orders of magnitude faster than regular DFT. Its high transferability was recently documented,<sup>51,53–62</sup> where an accuracy close to full DFT calculation was obtained for a number of molecular properties. In view of the current interest in sulfur chemistry and sulfur-containing biomolecules, this novel method was recently adopted to this element.<sup>51</sup>

**Radicals under Investigation.** We have computationally investigated the geometry and electronic composition of the model cation radicals derived from the compounds schematically represented in Chart 1. Importantly, structures **1** are methionine analogues, in which the methionine skeleton has been conformationally restricted within the backbone of a norbornane system. In contrast, structures **2** contain a regular, highly flexible Met residue.

All radical structures under investigation are displayed in Chart 2. Experimentally, the radicals **1a**<sup>+</sup>, **1b**<sup>+</sup>, **1bH**<sup>+</sup>, **2a**<sup>+</sup>, **2b**<sup>+</sup>, and **2d**<sup>+</sup> have been obtained through the •OH-radical-induced oxidation of *exo*-2-amino-*endo*-6-(methylthio)bicyclo[2.2.1]heptane-*endo*-2-carboxylic acid (**1a**), *endo*-6-(methylthio)bicyclo[2.2.1]heptane-*endo*-2-carboxylic acid (**1b**), methionine (**2a**), 4-(methylthio)butyric acid (**2b**), and methionine amide (**2d**).<sup>15,16,18,28,31,44</sup> Radicals **2e**<sup>+</sup> and **2f**<sup>+</sup> are derived from *N*-acetyl-L-methionine amide (**2e**) and *N*-acetyl-L-methionine *N'*-methylamide (**2f**). The formation of the first structure has been experimentally documented through pulse radiolysis.<sup>44</sup> Species **2g**<sup>+</sup> and **2h**<sup>+</sup> are models of radicals observed in synthetic poly-Gly-Met peptides,<sup>45</sup> whereas radical **2i**<sup>+</sup> is a poly-Gly-Met peptide radical adapted to the backbone conformation reflecting the native conformation of βAP.

Since higher level calculations of polypeptides would require an exceptional computation effort, we have limited the usage of “full-DFT” calculations accounting for water solvation, affecting the radical geometry, only to the radicals derived from compounds **1a–2f**.

All radicals were treated by the SCC-DFTB procedure, which was extensively tested for the reproducibility of higher level calculated geometries of S–S, S–N, and S–O three-electron-bonded radicals and radical-cations of small molecules. Most of our reference radicals have been thoroughly studied with different levels of theory, and are well qualified as benchmark systems for checking the accuracy of the new method.<sup>50,63–74</sup>

CHART 2<sup>a</sup>

The chemical formulas of the chosen reference radicals are listed in the first columns of Tables 2 and 3.

### Computational Methods

The density functional theory (DFT) calculations were performed for open-shell systems employing a commonly used, nonlocal hybrid functional, Becke3LYP,<sup>75</sup> which appears to be particularly useful for the computation of optimized molecular geometries<sup>68,70,76,77</sup> and spin densities.<sup>68,78–83</sup> The DFT optimizations and energy calculations were done utilizing the standard 6-31+G(d) and the 6-311+G(d) basis sets<sup>50,84–86</sup> offering the compromise between proper description of the anion-like species with a good performance at a modest computational cost, due to inclusion of diffuse and polarization functions on the heavy atoms only.<sup>85</sup> The radical structures were fully optimized by using the analytical gradient technique, and the nature of each located stationary point was checked by evaluating harmonic frequencies. The vibrational frequencies ( $\omega$ ), obtained from conventional harmonic normal-mode analysis of the respective geometries, are shown without any corrections. To account for the effect of the solvent on the geometry of the radicals the gas-phase structures were reoptimized in the integral equation formalism model (IEFPCM).<sup>87</sup> The theoretical estimates of both the location of the dominating absorption bands ( $\lambda_{\max}$ ) and an approximate description of the intensity (electronic oscillator strength  $f$ ) and electronic composition of the transition were obtained from time-dependent density functional response theory (TD-DFRT).<sup>88</sup> The TD-DFRT-B3LYP/6-311+G(d) calculations were done at the geometries obtained at the B3LYP/6-311+G(d) level. Additional attempts to calculate the UV transitions were done employing CIS calculations with the ZINDO/S semiempirical Hamiltonian.<sup>89–94</sup> Similarly to TD-DFRT, ZINDO/S calculations were done at the B3LYP/6-311+G(d)-optimized geometries.

Since the TD-DFRT method within Gaussian'98 does not collaborate with any implemented solvation models, we did attempt to estimate a solvatochromic shift on the low computing-

cost level, utilizing semiempirical<sup>94</sup> and molecular mechanics.<sup>95</sup> The general idea of our approach was partially adapted from the work of Karelson and Zerner,<sup>96</sup> who pointed out that the solvatochromic shift of the  $\pi \rightarrow \pi^*$  and the  $n \rightarrow \pi^*$  type absorption, which occurs in hydrogen-bonding solvents, depends on specific first-solvation-shell effects, and that calculation for “a supermolecule” containing a solute and explicit solvent molecules surrounded by continuum solvent gives better quantitative agreement with experiment than for a molecule of solute itself. In our approach, the B3LYP/6-311+G(d) geometries of radicals have been placed into a periodic box of water with constant dielectric permittivity. We used the three-site TIP3 model of Jorgensen et al.<sup>97</sup> for water in a box of 20 Å edge length (nearly five shells of water molecules), optimized employing the CHARMM<sup>95,98</sup> force field in its HyperChem implementations.<sup>99</sup> The single point ZINDO/S calculations were performed on the “supermolecule” containing the radical and its first hydration shell, surrounded by the rigid solvent, creating a field of classical potential, which perturbs the semiempirical Hamiltonian. Then, the expected solvatochromic shift was calculated from the equation  $\Delta UV_{\text{solv}} = \lambda_s - \lambda_g$ , where  $\lambda_s$  represents the lowest absorption band calculated with the ZINDO/S mixed model for the IEFPCM-B3LYP/6-311+G(d) optimized geometry, and  $\lambda_g$  is the lowest absorption band calculated with the ZINDO/S for the gas-phase B3LYP/6-311+G(d) level optimized geometry.

Simultaneous with the DFT calculation, the geometries of investigated radicals were optimized in the gas phase by the SCC-DFTB procedure. The SCC-DFTB model is derived from DFT by a second-order expansion of the DFT total energy with respect to the charge density fluctuation at given reference density. The SCC-DFTB method has been previously described in detail.<sup>51–58,60–62</sup>

The DFT calculations were performed with the Gaussian'98 suite of programs<sup>100</sup> in the Department of Pharmaceutical Chemistry of the University of Kansas and the Interdisciplinary Center for Mathematical and Computation Modeling University of Warsaw (ICM UW), Poland. The SCC-DFTB calculations were performed in ICM UW applying the dftb software developed at the University of Paderborn, Germany. The ZINDO/S and force field calculations were performed in the Institute of Nuclear Chemistry and Technology with use of the HyperChem 4.5<sup>101</sup> molecular modeling package. The input file structures of radicals were prepared on a PC computer, using the ISIS Draw 2.2.4<sup>102</sup> graphic program. The visualization of the computation results and the molecular fitting<sup>103</sup> were done with the gOpenMol 2.0<sup>104</sup> program. The file format conversions between modeling programs were done with the Babel 1.6<sup>105</sup> freeware program.

## Results

**Radicals from *exo*-2-Amino-*endo*-6-(methylthio)bicyclo[2.2.1]heptane-*endo*-2-carboxylic Acid (1a):** *Gas-Phase Geometry.* The fully relaxed gas-phase R and R1-geometry optimization of radical  $\mathbf{1a}^+$  leads to only one stable SO-bonded conformer (R refers to the B3LYP/6-31+G(d) level of theory and R1 to the B3LYP/6-311+G(d) level). Radical  $\mathbf{1a}^+$  adopts the  $\sigma^*$ -type arrangement with the odd electron on the  $\sigma^*$ -orbital, an antibonding combination of the sulfur  $3p_z$  orbital with the  $2p_\sigma$  orbital of the carboxylate anion (for R1, the dihedral angle  $\angle_{(O-C-O-S)} = 139.465^\circ$ ). The oxygen  $2p_\sigma$  orbital of  $\mathbf{1a}^+$  involved in SO bond formation possesses partial  $sp^3$  character ( $sp^{2.4}$ ), as evident from  $\angle_{(C-O-S)} = 114.823^\circ$  and  $r_{C-O-S} = \text{ca. } 1.27 \text{ \AA}$ ; instead, the length of the bond connecting the second

oxygen with the carboxylate carbon is  $r_{O=CO-S} = \text{ca. } 1.23 \text{ \AA}$ . The electronic structure of  $\mathbf{1a}^+$  can be approximately described as a two-center, three-electron ( $2c,3e$ )  $\sigma^*$ -type, with the computed oxygen–sulfur bond length  $r_{S-O} = 2.350 \text{ \AA}$ . Note that the relative position of the carboxylate group is maintained by an intramolecular hydrogen bond with the amino group with  $\angle_{(N-H-O)} = \text{ca. } 124.85^\circ$  and  $r_{H-O} = \text{ca. } 1.73 \text{ \AA}$ , ca. 60% of the sum of the van der Waals (vdw) radii of hydrogen and oxygen ( $2.9 \text{ \AA}$ <sup>41</sup>).

*Water-Phase Geometry.* The IEFPCM reoptimization of  $\mathbf{1a}^+$  results only in a small deformation of the gas-phase structure. (The root-mean-square distance (rmsd) of the Cartesian coordinates of all atoms in radical  $\mathbf{1a}^+$  vs its solvated form is equal to ca. 0.094 Å.) While for  $\mathbf{1a}_{\text{aq}}^+$   $r_{S-O} = 2.352 \text{ \AA}$  (nearly identical with the gas-phase structure),  $r_{H-O} (=2.01 \text{ \AA})$  is ca. 16% longer compared to the gas-phase structure.

*Spectral Properties.* The energy of the most intense one-electron transition in  $\mathbf{1a}^+$  (3.18 eV, 390 nm) calculated by TD-DFRT shows ca. 30 nm deviation from the experimental data obtained in aqueous solution (see Table 1).<sup>23</sup>

The calculated energy band is essentially described by a one-electron transition between the occupied  $\sigma$  and the singly occupied  $\sigma^*$  molecular orbitals, as evident by the weighting coefficients displayed in Table 1. The ZINDO/S calculation of the UV absorption of radicals  $\mathbf{1a}^+$  and  $\mathbf{1a}_{\text{aq}}^+$  predicts a hypsochromic shift of ca. 35 nm, bringing the computed bands very close to the experimentally observed value (see Table 1).<sup>23</sup> Radical  $\mathbf{1a}^+$  exhibits a vibrational frequency of ca.  $755 \text{ cm}^{-1}$ , which can be assigned to the S–O bond-stretching mode.

**Radicals from *endo*-6-(Methylthio)bicyclo[2.2.1]heptane-*endo*-2-carboxylic Acid (1b):** *Gas-Phase Geometry.* The fully relaxed gas-phase B3LYP/6-31G(d), R and R1-geometry optimization of radical  $\mathbf{1b}^+$  leads to one stable S–O-bonded conformer. Radical  $\mathbf{1b}^+$  adopts the  $\sigma^*$ -type arrangement with the odd electron on the  $\sigma^*$ -orbital, an antibonding combination of the sulfur  $3p_z$  orbital with the  $2p_\sigma$  orbital of the carboxylate anion (in R1, the torsion angle  $\angle_{(O-C-O-S)} = 161.953^\circ$ ). The oxygen  $2p_\sigma$  orbital of  $\mathbf{1b}^+$ , involved in S–O bond formation, is mainly of  $sp^2$  character ( $sp^{2.1}$ ), as evident from  $\angle_{(C-O-S)} = 119.032^\circ$  and  $r_{C-O-S} = \text{ca. } 1.30 \text{ \AA}$ ; instead, the length of the bond connecting the second oxygen with the carboxylate carbon is  $r_{O=CO-S}$  ca. 1.23 Å. The electronic structure of  $\mathbf{1b}^+$  can be approximately described as  $2c,3e$  with the computed oxygen–sulfur bond length  $r_{S-O} = 2.395 \text{ \AA}$  (R1). With the protonation of the carboxylate functionality ( $\mathbf{1bH}^+$ ) the  $r_{S-O}$  bond length increases up to 2.468 Å ( $\angle_{(C-O-S)} = 117.927^\circ$ ).

*Water-Phase Geometry.* The IEFPCM reoptimization of  $\mathbf{1b}^+$  results only in a small deformation of the gas-phase structure. (The root-mean-square distance (rmsd) of the Cartesian coordinates of all atoms in radical  $\mathbf{1b}^+$  vs its solvated form  $\mathbf{1b}_{\text{aq}}^+$  is equal to ca. 0.043 Å.) In  $\mathbf{1b}_{\text{aq}}^+$ ,  $r_{S-O} = 2.367 \text{ \AA}$ , which is ca. 12% shorter compared to the gas-phase structure.

*Spectral Properties.* The energy of the most intense one-electron transition in  $\mathbf{1b}^+$  (3.07 eV, 403 nm), calculated by TD-DFRT, shows an ca. 13-nm red shift compared to the experimental data in aqueous solution (390 nm; see Table 1).<sup>18</sup> The protonated form of radical  $\mathbf{1bH}^+$  exhibits two one-electron transitions (2.88 eV, 431 nm; 3.01 eV, 412 nm), which are by 41 and 22 nm red shifted compared to the experimental data.

The calculated energy bands are essentially described by a one-electron transition between the occupied  $\sigma$  and the singly occupied  $\sigma^*$  molecular orbitals, as evident by the weighting coefficients displayed in Table 1. The ZINDO/S calculation of the UV absorption of  $\mathbf{1b}^+/\mathbf{1b}_{\text{aq}}^+$  predicts a hypsochromic shift of



TABLE 1: Structural and Spectroscopic Parameters of Radicals Derived from Compounds 1a–2f<sup>a</sup>

	$r_{\text{SO}}$ [Å]	$\omega_{\text{SO}}$ [cm <sup>-1</sup> ]	$F$ [N cm <sup>-1</sup> ]	UV, $\lambda_{\text{max}}(\text{exptl})$ [nm]	UV, $\lambda_{\text{max}}(\text{calcd})$ [nm]	$f$	$c[\beta \rightarrow \beta^*]$
<b>1a<sup>•+</sup></b>	2.350	755	1.96		390 <sup>B</sup> 391 <sup>C</sup>	0.15	0.82 ( $\sigma \rightarrow \sigma^*$ )
<b>1a<sub>aq</sub><sup>•+</sup></b>	2.352			360 <sup>A</sup>	356 <sup>D</sup>		
<b>1b<sup>•</sup></b>	2.395	644	1.74		403 <sup>B</sup> 413 <sup>C</sup>	0.19	0.84 ( $\sigma \rightarrow \sigma^*$ )
<b>1b<sub>aq</sub><sup>•</sup></b>	2.367			390 <sup>E</sup>	385 <sup>D</sup>		
<b>1bH<sup>•+</sup></b>	2.468	683	1.35		431 <sup>B</sup> 411 <sup>B</sup>	0.04 0.04	0.83 ( $\sigma \rightarrow \sigma^*$ ) 0.68 ( $n \rightarrow \sigma^*$ )
<b>1bH<sub>aq</sub><sup>•+</sup></b>	2.460				411 <sup>B</sup> 321 <sup>C</sup>	0.12	0.76 ( $\sigma \rightarrow \sigma^*$ )
<b>1c<sup>•+</sup></b>	2.412	638	0.71		322 <sup>D</sup>		
<b>1c<sub>aq</sub><sup>•+</sup></b>	2.411				406 <sup>B</sup> 400 <sup>C</sup>	0.19	0.74 ( $\sigma \rightarrow \sigma^*$ )
<b>2a<sup>•+</sup></b>	2.386	741	1.82		380 <sup>D</sup>		
<b>2a<sub>aq</sub><sup>•+</sup></b>	2.391				426 <sup>B</sup> 451 <sup>C</sup>	0.23	0.73 ( $\sigma \rightarrow \sigma^*$ )
<b>2b<sup>•</sup></b>	2.460	541	0.87		322 <sup>D</sup>		
<b>2b<sub>aq</sub><sup>•</sup></b>	2.406			400 <sup>F</sup>	428 <sup>B</sup> 341 <sup>C</sup>	0.11	0.92 ( $\sigma \rightarrow \sigma^*$ )
<b>2bH<sub>aq</sub><sup>•+</sup></b>	2.499	652	0.70		386 <sup>D</sup>		
<b>2c<sup>•+</sup></b>	2.443	527	0.33		427 <sup>B</sup> 343 <sup>C</sup>	0.15	0.73 ( $\sigma \rightarrow \sigma^*$ )
<b>2c<sub>aq</sub><sup>•+</sup></b>	2.432				355 <sup>D</sup>		
<b>2d<sup>•+</sup></b>	2.619	468	0.38		455 <sup>B</sup> 418 <sup>C</sup>	0.07	0.94 ( $\sigma \rightarrow \sigma^*$ )
<b>2e<sub>(1,6)</sub><sup>•+</sup></b>	2.411	506	0.42		408 <sup>B</sup> 333 <sup>C</sup>	0.13	0.93 ( $\sigma \rightarrow \sigma^*$ )
<b>2e<sub>(1,6)aq</sub><sup>•+</sup></b>	2.399			390 <sup>G</sup>	321 <sup>D</sup>		
<b>2e<sub>(1,7)</sub><sup>•+</sup></b>	2.438	513	0.43		453 <sup>B</sup> 394 <sup>B</sup>	0.06 0.01	0.94 ( $\sigma \rightarrow \sigma^*$ ) 0.96 ( $n \rightarrow \sigma^*$ )
<b>2f<sub>(1,6)</sub><sup>•+</sup></b>	2.400	548	0.62		412 <sup>C</sup> 416 <sup>B</sup> 407 <sup>C</sup>	0.12	0.92 ( $\sigma \rightarrow \sigma^*$ )
<b>2f<sub>(1,6)aq</sub><sup>•+</sup></b>	2.405				335 <sup>D</sup>		

<sup>a</sup> Key: (A) Observed in aqueous solution. Data redeconvoluted compared to the original presented in ref 23. (B) TD-DFRT-R1/R1. (C) ZINDO/S/R1. (D) ZINDO/S//IEFPCM-R1 in the 20 Å edge length H<sub>2</sub>O periodic box, mixed-mode. (E) Observed in aqueous solution. Reference 18. (F) Observed in aqueous solution. Reference 16. (G) Observed in aqueous solution. Reference 44.

ca. 28 nm, bringing the computed band to a little below the experimentally observed value (see Table 1).<sup>18</sup> Radicals **1b<sup>•</sup>** and **1bH<sup>•+</sup>** exhibit vibrational frequencies of ca. 644 and 683 cm<sup>-1</sup>, respectively, which can be assigned to the S–O bond-stretching modes.

**Radicals Derived from *endo*-6-(Methylthio)bicyclo[2.2.1]-heptane-*endo*-2-carboxylic Acid Amide (1c):** *Gas-Phase Geometry.* The fully relaxed gas-phase B3LYP/6-31G(d), R and R1-geometry optimization of radical **1b<sup>•+</sup>** leads to only one stable SO-bonded conformer. Radical **1c<sup>•+</sup>** adopts the  $\sigma^*$ -type arrangement with the odd electron on the  $\sigma^*$ -orbital, an antibonding combination of the sulfur 3p<sub>z</sub> orbital with the 2p<sub>o</sub> orbital of the carbonyl oxygen of carboxylate anion ( $\angle_{\text{N-C-O-S}} = 151.531^\circ$ ). The oxygen 2p<sub>o</sub> orbital of **1c<sup>•+</sup>**, involved in S–O bond formation, is mainly of sp<sup>2</sup> character (sp<sup>~2.2</sup>), as evident from  $\angle_{\text{C-O-S}} = 117.525^\circ$  and  $r_{\text{C-O-S}} = \text{ca. } 1.25 \text{ \AA}$ , where the length of the bond connecting the amide nitrogen with the carbonyl carbon,  $r_{\text{N=COS}}$ , is ca. 1.34 Å. The electronic structure of **1c<sup>•+</sup>** can be approximately described as 2c,3e with the computed oxygen–sulfur bond distance  $r_{\text{S-O}} = 2.412 \text{ \AA}$ .

*Water-Phase Geometry.* The IEFPCM reoptimization of **1c<sup>•+</sup>** (Figure 1) results only in a small deformation of the gas-phase structure. (The rmsd of the Cartesian coordinates of all atoms in radical **1c<sup>•+</sup>** vs its solvated form **1c<sub>aq</sub><sup>•+</sup>** is equal to ca. 0.046 Å.) In **1c<sub>aq</sub><sup>•+</sup>**,  $r_{\text{S-O}} = 2.411 \text{ \AA}$ , i.e., a little shorter than that calculated for the gas-phase structure **1c<sup>•+</sup>**.

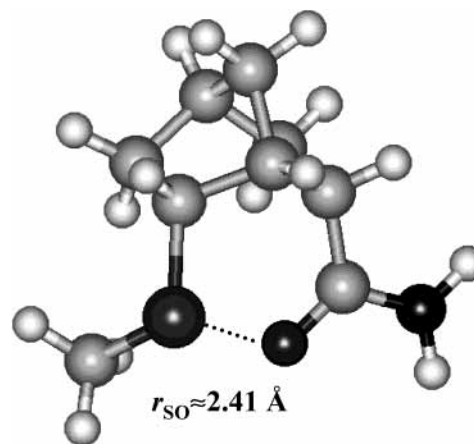
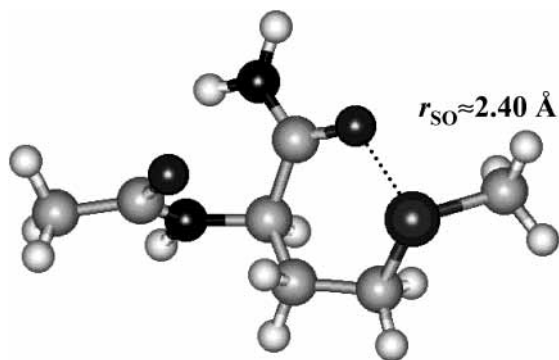


Figure 1. The DFT-IEFPCM calculated geometry of radical **1c<sub>aq</sub><sup>•+</sup>**.

*Spectral Properties.* The TD-DFRT calculation predicts an energy of 3.02 eV (411 nm) for the most intense one-electron transition in **1c<sup>•+</sup>**. The calculated energy is for a one-electron transition between the occupied  $\sigma$  and the singly occupied  $\sigma^*$  molecular orbitals, as evident from the weighting coefficients displayed in Table 1. Radical **1c<sup>•+</sup>** exhibits a vibrational frequency of ca. 638 cm<sup>-1</sup>, which can be assigned to the S–O bond-stretching mode.



**Figure 2.** The DFT-IEFPCM calculated geometry of radical  $2e_{aq(1,6)}^{+}$ .

**Radicals Derived from L-Methionine, 4-(Methylthio)butyric Acid, and Their Respective Amides (2a–d).** In principle, radicals  $2a^{+}-c^{+}$  can be derived from radicals  $1a^{+}-c^{+}$  by relief of the conformational constraints imposed through the norbornane skeleton. This results in a substantial increase of the computed oxygen–sulfur bond lengths,  $r_{S-O}$ , in radicals  $2a^{+}-c^{+}$ . Such increases of the  $r_{S-O}$  bond lengths cause a decrease of the energies for vertical one-electron transitions and the S–O bond-stretching modes. The presence of an extra positive charge on the amino group of radical  $2d^{2+}$  pronounces these effects (see Table 1). Similar to  $1a^{+}-1^{+}$ , the electronic structures of radicals  $2a^{+}-d^{2+}$  can be described as  $2c,3e$  of a pyramidal  $\sigma^*$ -type S–O-bonded arrangement. The optical absorption bands in all these radical cations are attributable to a moderately strong  $\sigma \rightarrow \sigma^*$  transition in the  $\beta$ -space (see Table 1).

**Water-Phase Geometries.** The IEFPCM reoptimization of radicals  $2a^{+}-2c^{+}$  results in a small deformation of their gas-phase structures. The rmsd of the Cartesian coordinates of all atoms in the radicals are equal to ca. 0.193, 0.033, 0.078, and 0.077 Å for pairs  $2a^{+}/2a_{aq}^{+}$ ,  $2b^{+}/2b_{aq}^{+}$ ,  $2bH^{+}/2bH_{aq}^{+}$ , and  $2c^{+}/2c_{aq}^{+}$ , respectively. For all radicals, except  $2a^{+}$ , solvation results in a decrease of the  $r_{S-O}$  length (see Table 1).

**Radicals Derived from N-Acetyl-L-methionine Amide (2e) and N-Acetyl-L-methionine N'-Methylamide (2f).** The geometries of the SO-bonded cation radicals  $2e^{+}$  and  $2f^{+}$  derived from N-acetyl-L-methionine amide and N-acetyl-L-methionine N'-methylamide were computed on the basis of assumed similarities with the geometries of radicals  $1e^{+}$  and  $2e^{+}$ . Thus, in the initial structures of radicals  $2e^{+}$  and  $2f^{+}$ , prior to optimization, the 4-(methylthio)butyric acid chain was set in the conformation corresponding to the conformation of radical  $1e^{+}$ , then freely optimized on the R1-level. It resulted in optimized structures, which reflect the chemical bonding in  $1e^{+}$  (see Table 1). For the radicals derived from  $2e$  and  $2f$  not only the 1,6-type of S–O bonding but also the 1,7-type may exist. In the following, a subscript (x,y) added to the radical specification indicates the type and ring size of the respective S–O bond. We performed a fully relaxed energy minimization of  $2e^{+}$  in the vicinity of a hypothetical 1,7-type S–O-bonded structure, obtaining radical  $2e_{(1,7)}^{+}$ , which is ca. 3.1 kcal mol<sup>-1</sup> higher in energy than  $2e_{(1,6)}^{+}$ . Similarly to the radicals characterized above, the IEFPCM reoptimization of radicals  $2e_{(1,6)}^{+}$  and  $2f_{(1,6)}^{+}$  results only in a small deformation of their gas-phase structures. The rmsd of the Cartesian coordinates of all atoms in the radicals are equal to ca. 0.096 and 0.017 Å for pairs  $2e_{(1,6)}^{+}/2e_{(1,6)aq}^{+}$  and  $2f_{(1,6)}^{+}/2f_{(1,6)aq}^{+}$ , respectively. The geometry of radical  $2e_{(1,6)aq}^{+}$  is shown in Figure 2.

**Application of the SCC-DFTB Method.** To test the performance of the SCC-DFTB method we calculated relative

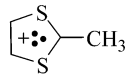
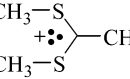
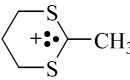
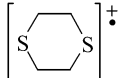
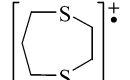
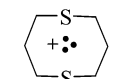
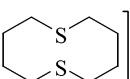
energies and geometries for a test set of 30 molecules, including radicals  $1a^{+}-2f^{+}$ , which covers the 1e-oxidized sulfur in almost all three-electron bond systems, which can be expected in biological systems. These include S–O, S–S, and S–N bonded radical and radical–cationic intermediates. We compared the performance of the approximate methods AM1, PM3 and self-consistent charge, density-functional tight-binding (SCC-DFTB) to density-functional theory (DFT), Hartree–Fock (HF), MP2, and QCISD. Most of the Cartesian coordinates of the reference molecules were taken from the literature. If the original Cartesian coordinates were not available, we recalculated them based on the originally published level of theory, whenever possible. Tables 2, 3, and 4 list the results of the SCC-DFTB calculations together with those of AM1, PM3, ab initio, and DFT calculations.

The SCC-DFTB method yields qualitatively correct geometries, which compare better to the DFT-computed than to the ab initio-computed results. The SCC-DFTB-derived three-electron bond lengths compare well with the corresponding values obtained with higher level theories, showing small deviations in the range of –3.1 to 6.5%. The SCC-DFTB method fails only in two cases predicting the S–N bond length in 3-(methylthio)propylamine-derived radical cations with a relative error of ca. –15%. The semiempirical methods AM1 and PM3 show systematic deficiencies underestimating the three-electron bond lengths by –9 to –36%.

Generally all approximate methods (SCC-DFTB, AM1, PM3) reproduce the energetic ordering of the three-electron-bonded conformers quite well, correctly picking the lowest energy conformer (see Table 4). However, the AM1 and PM3 methods substantially overestimate the conformational energy differences of the S–S-bonded systems (by ca. 10 to 31 kcal mol<sup>-1</sup>), whereas the SCC-DFTB method shows 2–4 kcal mol<sup>-1</sup> discrepancy compared to the DFT values (see Table 4). We found that the SCC-DFTB gas-phase calculations have difficulties with the correct description of radicals  $1a^{+}$  and  $2a^{+}$  derived from the zwitterionic amino acids  $1a$  and  $2a$ . In both cases, the acidic proton is bound to the carboxylate instead of the amino group. For both  $1a^{+}$  and  $2a^{+}$ , this results in exceptionally high (0.217 and 0.234 Å, respectively) root-mean-square distances (rmsd) of the Cartesian coordinates of all atoms compared to the DFT-calculated structures. However, we know that the majority of gas-phase calculations point to the zwitterionic form of an amino acid as its isomer of higher energy; thus, we cannot expect the SCC-DFTB method to perform much better. On the other hand, for the majority of radicals the rmsd's of Cartesian coordinates of all atoms are on the level comparable to that observed for the DFT-calculated vs the DFT-IEFPCM-calculated solvated forms.

**Radicals Derived from Model Poly-Gly-Met Peptides and  $\beta$ AP.** Encouraged by the good performance of the SCC-DFTB method we utilized it for the calculation of geometries of model radicals  $2g^{+}$ ,  $2h^{+}$ , and  $2i^{+}$  derived from (Gly)<sub>n</sub>-Met-(Gly)<sub>m</sub>-type peptides.<sup>45</sup> For radicals  $2g^{+}$  and  $2h^{+}$  the initial structures were set as a 3.6<sub>13</sub>-helix. A slightly different approach was utilized for radical  $2i^{+}$ , for which the initial structure was derived from the published solution structure of  $\beta$ AP1–40, previously obtained by distance geometry calculation employing NMR-derived NOE restraints.<sup>40</sup> To obtain an initial structure of  $2i^{+}$  the structure of  $\beta$ AP1–40 was truncated to  $\beta$ AP30–37, then all residues except Met<sup>35</sup> were mutated to Gly. Initially, the  $\beta$ AP-like secondary structure of  $2i^{+}$  was preserved by “freezing” of the internal coordinates of the atoms of the peptide backbone (except that belonging to the Met<sup>35</sup> and Ile<sup>31</sup>Gly

**TABLE 2: SCC-DFTB Calculated Bond Lengths, in Å, of the (S..S)-Bonded Radicals in Comparison to the Literature Data Obtained by Using ab Initio/DFT Methods and Root-Mean-Square Distance (rmsd), in Å, of the Cartesian Coordinates of All Atoms in the SCC-DFTB vs ab Initio/DFT Optimized Structures<sup>a</sup>**

Radical	$r_{S..S}$ Ref.	$r_{S..S}$ DFTB	$rmsd$ DFTB	$r_{S..S}$ AM1	$rmsd$ AM1	$r_{S..S}$ PM3	$rmsd$ PM3	Reference Method	
$H_2S..SH_2^+$	2.89 2.78 2.73 2.84	2.80		2.11		2.05		BP86/TZ2P <sup>B</sup> PW91/TZ2P <sup>B</sup> MP2/6-311++G(2df,2pd) <sup>B</sup> MP2/6-31(d) <sup>C</sup>	
$Me_2S..SMe_2^+$	2.84 2.80	2.78	0.056 <sup>A</sup> 0.044 <sup>A</sup>	2.27	0.150 <sup>A</sup> 0.137 <sup>A</sup>	2.11	0.294 <sup>A</sup> 0.307 <sup>A</sup>	HF/6-31G(d) <sup>C</sup> MP2/6-31G(d) <sup>C</sup>	
$Et_2S..SEt_2^+$	2.87	2.80	0.395 <sup>A</sup>	2.05	0.480 <sup>A</sup>	2.05	0.480 <sup>A</sup>	C <sub>2</sub> – conformer, HF/6-31G(d) <sup>C</sup>	
	2.62	2.79	0.074	2.39	0.086	2.39	0.086	BHLLYP/6-311+G(d,p) <sup>D</sup>	
	2.69	2.78	0.093	2.40	0.154	2.21	0.351	BHLLYP/6-311+G(d,p) <sup>D</sup>	
	2.68	2.76	0.061	2.41	0.118	2.23	0.202	BHLLYP/6-311+G(d,p) <sup>D</sup>	
	2.70 3.42 3.34	2.75 3.44 3.43	0.058 0.051 0.329	2.35 3.29 3.29	0.078 0.224 0.149	2.34 3.34 3.34	0.088 0.324 0.111	Boat structure, BHLLYP/6-311+G(d,p) <sup>D</sup> Chair structure, BHLLYP/6-311+G(d,p) <sup>D</sup> Twist structure, BHLLYP/6-311+G(d,p) <sup>D</sup>	
		2.70 3.55	2.73 3.47	0.051 0.066	2.27 3.42	0.121 0.306	2.18 3.53	0.156 0.272	All cis structure, BHLLYP/6-311+G(d,p) <sup>D</sup> All trans structure, BHLLYP/6-311+G(d,p) <sup>D</sup>
			2.73	2.76	0.048	2.19	0.140	2.05	0.165
	2.76 5.55	2.77 5.55	0.076 0.051	2.17 5.26	0.185 0.106	2.05 5.26	0.835 0.107	All cis structure, BHLLYP/6-311+G(d,p) <sup>D</sup> All trans structure, BHLLYP/6-311+G(d,p) <sup>D</sup>	

<sup>a</sup> Key: (A) the reference DFT/ab initio Cartesian coordinates have been recalculated (see text); (B) ref 69; (C) ref 115; (D) ref 74.

residues), then pre-optimized. Finally, after removal of all constraints, the molecule was freely optimized. Fully relaxed SCC-DFTB gas-phase geometry optimizations of radicals  $2g^{*+}$ ,  $2h^{*+}$ , and  $2i^{*+}$  in the vicinity of hypothetical 1,(6+3n)- and 1,(7+3n)-type S–O-bonded structures (here, any transient sulfur–oxygen association would be of the 1,(6+3n)-type with amide bonds C-terminal of Met and the 1,(7+3n)-type with amide bonds N-terminal of Met ( $n = 0, 1, 2, \dots$ )), obtained by rotation of the Met-residue along its C<sub>α</sub>–C<sub>β</sub> bond, led to the following radicals (in the case of close distances of the Met S atom to more than one peptide bond oxygen, the subscript defines all possible S–O bond types):  $2g_{(1,6;1,15)}^{*+}$ ,  $2g_{(1,13)}^{*+}$ ,  $2h_{(1,6;1,15)}^{*+}$ ,  $2h_{(1,13)}^{*+}$ ,  $2i_{(1,16)}^{*+}$ , and  $2i_{(1,6)}^{*+}$ . Their physicochemical properties are summarized in Table 5. The structures of radicals  $2g_{(1,6;1,15)}^{*+}$ ,  $2g_{(1,13)}^{*+}$ ,  $2i_{(1,16)}^{*+}$ , and  $2i_{(1,6)}^{*+}$  are shown in Figures 3 and 4.

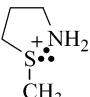
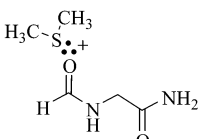
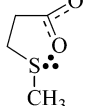
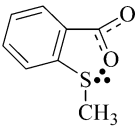
## Discussion

**The Sulfur–Oxygen Bond, Geometry, and Physicochemical Properties.** Our work demonstrates the possibility for formation of S–O bonds between an oxidized Met sulfur and the oxygen of carboxylate and amide functionalities. All the DFT-calculated radical structures are characterized by two-center, three-electron ( $2\sigma/1\sigma^*$ ) bonds and can, therefore, be represented by the notation S..O; however, their geometries vary based on the local chemical environments. The variation of the S–O bond length ( $r_{SO} = 2.35\text{--}2.62$  Å) is reflected in a change of  $\lambda_{max}$  for the lowest energy optical band. For all

investigated radicals this is assigned to a moderately strong  $\sigma \rightarrow \sigma^*$  transition in the  $\beta$ -space. The notable decrease of the energy of the  $\sigma \rightarrow \sigma^*$  transition with the increase of the S..O bond length is in accord with the intuitive interpretation of data for the S..S bond,<sup>63</sup> which can be extended to the S..O bond.<sup>73</sup> The optical absorption energy of a three-electron bond depends on the relative position of the  $\sigma$  and  $\sigma^*$  levels, and one parameter affecting the latter would be the extent of p-orbital overlap. An increase of p-overlap is associated with a lowering of the  $\sigma$ -level, and a rise of the  $\sigma^*$ -level, and, consequently, an increasing  $\sigma/\sigma^*$  separation. Thus, an increasing overlap results in a blue shift, while a decreasing overlap results in a red shift of the absorption. Obviously, p-overlap is expected to be a function of the internuclear distances, i.e., the bond lengths. This phenomenon is illustrated by the relationship that emerges on plotting the TD-DFT-calculated energies of the vertical transition against the RI-optimized lengths of the (S..O) bonds in radicals  $1a^{*+} - c^{*+}$  and  $2a^{*+} - f^{*+}$  (see Figure 5). The useful relationship shown in Figure 5 can be utilized for the rationalization of the observed discrepancies between the TD-DFT-calculated and the experimentally measured UV-absorption bands. The TD-DFT-calculated  $\lambda_{max}$  are somehow red-shifted compared to the experimental values obtained in water (see column 5 in Table 1). As the presence of water results in “solvation-induced” shortening of  $r_{SO}$  (see column 2 in Table 1), this should generate a negative solvatochromic shift, as experimentally observed.

The difference between the energies of the lowest absorption bands in radicals  $1a^{*+}$  and  $1b^{\bullet}$  can be explained by the extent of

**TABLE 3: SCC-DFTB Calculated Bond Lengths, in Å, of the (S··N)- and (S··O)-Bonded Radicals in Comparison to the Data Obtained by Using ab Initio/DFT Methods and Root-Mean-Square Distance (rmsd), in Å, of the Cartesian Coordinates of All Atoms in the SCC-DFTB vs ab Initio/DFT Optimized Structures<sup>a</sup>**

Radical	$r_{S··X}^A$ Ref.	$r_{S··X}^A$ DFTB	$rmsd$ DFTB	$r_{S··X}^A$ AM1	$rmsd$ AM1	$r_{S··X}^A$ PM3	$rmsd$ PM3	Reference Method
H <sub>2</sub> S··NH <sub>3</sub> <sup>+</sup>	2.46	2.50	0.227 <sup>B</sup>	1.79	0.341 <sup>B</sup>	1.87	0.331 <sup>B</sup>	HF/6-311G(d,p) <sup>C</sup>
	2.54		0.197 <sup>B</sup>		0.364 <sup>B</sup>		0.351 <sup>B</sup>	B3LYP/6-311G(d,p) <sup>C</sup>
	2.44		0.246 <sup>B</sup>		0.340 <sup>B</sup>		0.333 <sup>A</sup>	QCISD/6-311G(d,p) <sup>C</sup>
	2.52	2.24	na	1.94	na	1.89	na	<sup>3</sup> E – conformer, HF/6-311G(d,p) <sup>C</sup>
	2.58							<sup>3</sup> E – conformer, B3LYP/6-311G(d,p) <sup>C</sup>
	2.54	2.22	na	1.94	na	1.89	na	E <sub>3</sub> – conformer, HF/6-311G(d,p) <sup>C</sup>
	2.59							E <sub>3</sub> – conformer, B3LYP/6-311G(d,p) <sup>C</sup>
Me <sub>2</sub> S··OH <sub>2</sub> <sup>+</sup>	2.88	2.88	0.227 <sup>B</sup>	1.91	0.341 <sup>B</sup>	1.86	0.331 <sup>B</sup>	HF/6-31G(d) <sup>D</sup>
Me <sub>2</sub> S··OH	2.05	2.05	0.344 <sup>B</sup>	1.73	0.293 <sup>B</sup>	1.73	0.293 <sup>B</sup>	MP2/6-31+G(2d) <sup>E</sup>
	2.48	2.54	0.237 <sup>B</sup>	1.83	0.300 <sup>B</sup>	1.82	0.268 <sup>B</sup>	B3LYP/6-31G(d) <sup>F</sup>
	2.41	2.46	0.049	1.79	0.570	1.78	0.576	<sup>3</sup> E – conformer, B3LYP/6-31+G(d) <sup>G</sup>
	2.41	2.44	0.050	1.79	0.516	1.78	0.520	E <sub>3</sub> – conformer, B3LYP/6-31+G(d) <sup>G</sup>
	2.39	2.44	0.027	1.81	0.358	1.79	0.333	B3LYP/6-311+G(d) <sup>G</sup>
(AcCys(Me)NMe <sub>2</sub> ) <sup>•+</sup>	2.42	2.50	0.008	1.85	0.330	1.83	0.348	B3LYP/6-31+G(d) <sup>H</sup>
<b>1a<sup>•+</sup></b>	2.35	2.48	0.217	1.80	0.153	1.80	0.142	B3LYP/6-311+G(d) <sup>I</sup>
<b>1b<sup>•</sup></b>	2.40	2.45	0.075	1.77	0.167	1.77	0.176	B3LYP/6-311+G(d) <sup>I</sup>
<b>1bH<sup>•+</sup></b>	2.47	2.50	0.054	1.86	0.144	1.83	0.152	B3LYP/6-311+G(d) <sup>I</sup>
<b>1c<sup>•+</sup></b>	2.41	2.48	0.083	1.83	0.136	1.82	0.149	B3LYP/6-311+G(d) <sup>I</sup>
<b>2a<sup>•+</sup></b>	2.39	2.51	0.234	1.80	0.242	1.80	0.230	B3LYP/6-311+G(d) <sup>I</sup>
<b>2b<sup>•</sup></b>	2.46	2.49	0.071	1.77	0.272	1.77	0.320	B3LYP/6-311+G(d) <sup>I</sup>
<b>2bH<sup>•+</sup></b>	2.50	2.51	0.059	1.87	0.177	1.83	0.199	B3LYP/6-311+G(d) <sup>I</sup>
<b>2c<sup>•+</sup></b>	2.44	2.49	0.071	1.84	0.169	1.82	0.210	B3LYP/6-311+G(d) <sup>I</sup>
<b>2d<sup>•2+</sup></b>	2.62	2.54	0.101	1.87	0.373	1.79	0.415	B3LYP/6-311+G(d) <sup>I</sup>
<b>2e<sup>•+</sup></b> <sub>(1,6)</sub>	2.41	2.52	0.636	1.83	0.614	1.81	0.535	B3LYP/6-311+G(d) <sup>I</sup>
<b>2e<sup>•+</sup></b> <sub>(1,7)</sub>	2.44	2.53	0.207	1.82	1.022	1.81	1.047	B3LYP/6-311+G(d) <sup>I</sup>
<b>2f<sup>•+</sup></b> <sub>(1,6)</sub>	2.40	2.49	0.825	1.83	0.836	1.81	0.746	B3LYP/6-311+G(d) <sup>I</sup>

<sup>a</sup> Key: (A) X = O or N. (B) The reference DFT/ab initio Cartesian coordinates have been recalculated (see text). (C) Reference 68. (D) Reference 116. (E) Reference 117. (F) Reference 71. (G) Reference 73. (H) Reference 118. (I) This work.

p-orbital overlap leveraging the relative position of the  $\sigma$  and  $\sigma^*$  levels. However, the simple dependence of the extent of p-orbital overlap on the S–O internuclear distance change cannot explain the entire observed effect. We believe that the relative increase of the separation of  $\sigma$  and  $\sigma^*$  levels in **1a<sup>•+</sup>**/**1a<sup>•+</sup>**<sub>aq</sub> compared with **1b<sup>•</sup>**/**1b<sup>•</sup>**<sub>aq</sub> is due to the participation of electron density from the p <sub>$\pi$</sub> -orbital<sup>106</sup> of the carboxylate group in the S–O bond. Thus, the comparison of the total spin density in **1a<sup>•+</sup>**<sub>aq</sub> and **1b<sup>•</sup>**<sub>aq</sub>, shown in Figure 6, reveals a remarkable shift toward the thioether sulfur in **1a<sup>•+</sup>**<sub>aq</sub>. The  $\pi$ -electron may participate in the S–O bond of **1a<sup>•+</sup>**<sub>aq</sub> since the 2p <sub>$\sigma$</sub>  and 2p <sub>$\pi$</sub>  orbitals of carboxylate partially overlap. To form an S–O bond in **1a<sup>•+</sup>**/**1a<sup>•+</sup>**<sub>aq</sub>, the 2p <sub>$\sigma$</sub> -orbital of the carboxylate oxygen in **1a<sup>•+</sup>**<sub>aq</sub> is ca. 37° bent from the plane of the carboxylate group, compared to ca. 14° for **1b<sup>•</sup>**<sub>aq</sub>. Geometrically, this results in a ca. 2.5 times higher projection of the angular part of the 2p <sub>$\sigma$</sub> -orbital on the direction of the p <sub>$\pi$</sub> -orbital, which is perpendicular to the plane of the carboxylate.

Such extorted orbital arrangement in **1a<sup>•+</sup>** is forced by the rigid, norbornane-type “frame” of the methionine chain and the formation of the intramolecular hydrogen bond between the second carboxylate oxygen and the nitrogen of the amino functionality, which “turns” the plane of the carboxylate. The energy of the intramolecular H-bond may be estimated based on the hydrogen–oxygen distance,  $r_{HO}$ , using the extrapolation formula introduced by Krygowski et al.,<sup>107</sup>  $E = -110.7 \exp\{-4.012(0.975 - r_{HO})\}$  kcal mol<sup>-1</sup>. Here,  $E$  represents the gain of energy as the oxygen atom approaches a proton of the amino function from infinity to the equilibrium distance, giving ca. -5.8 kcal mol<sup>-1</sup> for radical **1a<sup>•+</sup>** and ca. -1.75 kcal mol<sup>-1</sup> for its hydrated form **1a<sup>•+</sup>**<sub>aq</sub>.

Importantly, the formation of different S–O bonds may result not only in different UV-absorption spectra but also in different reactivities of the radical transients and, consequently, in the formation of different final products. For example, the geometry of the SO bond may determine the reduction potential of the



**TABLE 4: Conformational Energies (kcal mol<sup>-1</sup>) of Three-Electron-Bonded Radicals for the DFT, SCC-DFTB, AM1, and PM3 Calculations<sup>a</sup>**

Radical	Conformer/ Isomer	DFT	SCC-DFTB	AM1	PM3
	Boat	0.0 <sup>A</sup>	0.0	0.0	0.0
	Chair	0.5 <sup>A</sup>	2.3	18.0	14.6
	Twist	4.4 <sup>A</sup>	2.3	18.0	14.6
	"All cis"	0.0 <sup>A</sup>	0.0	0.0	0.0
	"All trans"	17.8 <sup>A</sup>	14.3	32.5	31.6
	"All cis"	0.0 <sup>A</sup>	0.0	0.0	0.0
	"All trans"	23.4 <sup>A</sup>	19.8	43.5	54.5
	<sup>3</sup> E	0.0 <sup>B</sup>	0.0	0.0	0.0
	E <sub>3</sub>	0.3 <sup>B</sup>	0.3	0.1	0.2
	<sup>3</sup> E	0.1 <sup>C</sup>	0.0	0.0	0.0
	E <sub>3</sub>	0.0 <sup>C</sup>	0.5	3.9	0.03
<b>2e<sup>•+</sup></b>	SO <sub>(1,6)</sub>	0.0	0.0	0.0	0.0
	SO <sub>(1,7)</sub>	3.1	4.1	2.5	6.0

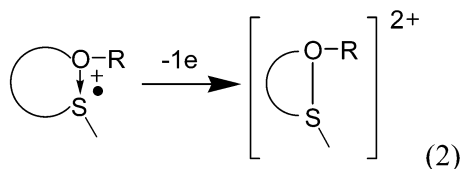
<sup>a</sup> Key: (A) BHHLYP/6-311+G(d,p), ref 74. (B) B3LYP/6-311G(d,p), ref 68. (C) B3LYP/6-31+G(d), ref 73.

**TABLE 5: Physico-Chemical Properties of Radicals Derived from Compounds 2g–2i<sup>a</sup>**

	$r_{SO}^A$ [Å]	UV, $\lambda_{max}^B$ [nm]	$E_{hyd}^C$ [kcal mol <sup>-1</sup> ]	log $P^D$
<b>2g<sup>•+</sup></b> <sub>(1,6;1,15)</sub>	2.65	627	-14.98	-3.61
	2.75	406		
<b>2g<sup>•+</sup></b> <sub>(1,13)</sub>	2.46	505	-15.39	-3.61
		473		
<b>2h<sup>•+</sup></b> <sub>(1,6;1,15)</sub>	2.69	515	-11.25	-3.38
	2.75	490		
<b>2h<sup>•+</sup></b> <sub>(1,13)</sub>	2.30	401	-10.25	-3.38
		360		
<b>2i<sup>•+</sup></b> <sub>(1,16)</sub>	2.449	634	-17.12	-4.20
<b>2i<sup>•+</sup></b> <sub>(1,6)</sub>	2.511	415	-22.29	-4.29
		404		

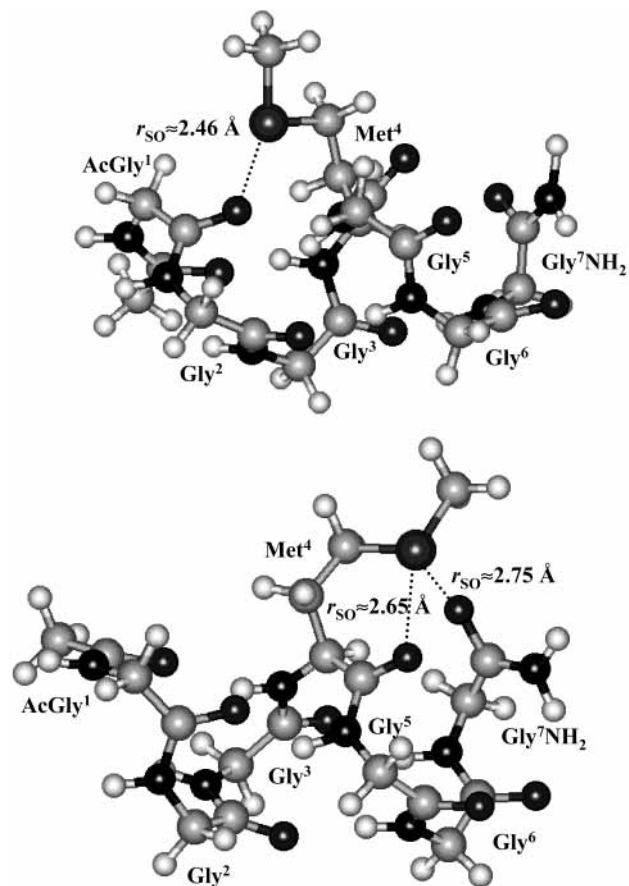
<sup>a</sup> Key: (A) ZINDO/S//SCC-DFTB. (B) ZINDO/S//SCC-DFTB. (C) QSAR calculated for "neutral" compounds of respective peptide radical conformation, ref 119. (D) QSAR calculated for "neutral" compounds of respective peptide radical conformation, refs 120 and 121.

thioether sulfur. As the energy of the  $\sigma^*$  orbital of the 3e/2c system is quantitatively correlated with the  $\sigma/\sigma^*$  separation, which itself is reflected in the  $\lambda_{max}$  for the electronic transition  $\sigma \rightarrow \sigma^*$ , one should expect a quantitative correlation between the  $\lambda_{max}$  data and the orbital energy of  $\sigma^*$ . By analogy to the S–S-bonded systems,<sup>108</sup> the latter is related to the ionization potential of reaction 2. More importantly, the energies of  $\sigma^*$



will affect the first ionization according to reaction 1. Moreover, if the solvation energies of reactants and products of reactions 1 and 2 are more or less constant, then even quantitative correlations between vertical ionization energies and reduction peak potentials might be possible.<sup>109,110</sup>

**Formation of Multiple Structures of S–O-Bonded Radicals in Peptides.** In peptides, the oxidized sulfur center can associate with various peptide bond carbonyl oxygens, forming

**Figure 3.** The SCC-DFTB calculated geometries of radicals **2g<sup>•+</sup>**<sub>(1,6;1,15)</sub> (lower panel) and **2g<sup>•+</sup>**<sub>(1,13)</sub> (upper panel).

an S–O-bonded configuration. However, not all of the structures are equally probable. For example, for the simplest Met-containing peptide *N*-AcMetNH<sub>2</sub> (**2e**) DFT calculations show the possibility for formation of at least two S–O-bonded radicals through 1,6- and 1,7-cyclization, respectively, with the 1,6-type bonded species **2e<sup>•+</sup>**<sub>(1,6)</sub> lying ca. 3.1 kcal mol<sup>-1</sup> below **2e<sup>•+</sup>**<sub>(1,7)</sub>. We believe that numerous local and global forces<sup>111–114</sup> stabilizing the secondary and tertiary structure of proteins may also influence the formation of S–O-bonded species. Even one specific interaction comparable to the energy of one H-bond in radical **1a<sup>•+</sup>** may provide the energy gain sufficient for quite dramatic changes of the properties of particular S–O-bonded species or the selectivities of their formation.

The SCC-DFTB calculations for radicals derived from model peptides **2g**, **2h**, and **2i** show that the secondary structures of the peptides may support the formation of particular S–O-bonded radicals. The "pure"  $\alpha$ -helical conformation of peptides **2g** and **2h** allows the 1,6-, 1,15-, and 1,13-type cyclization whereas in peptide **2i** (the model of  $\beta$ AP) the 1,16- and 1,6-type cyclization may occur. The SCC-DFTB results suggest that in the gas phase the isomer **2i<sup>•+</sup>**<sub>(1,6)</sub> is thermodynamically more stable than **2i<sup>•+</sup>**<sub>(1,6)</sub>. Also QSAR calculations suggest that **2i<sup>•+</sup>**<sub>(1,6)</sub> should be a preferable isomer of **2i<sup>•+</sup>** in aqueous solution. However, the formation of **2i<sup>•+</sup>**<sub>(1,6)</sub> may be kinetically difficult since it requires a substantial rearrangement of the Met side chain compared to the native conformation of  $\beta$ AP. Therefore, molecular modeling shows a negligible propensity for the formation of **2i<sup>•+</sup>**<sub>(1,6)</sub> in the representative congeners of  $\beta$ AP.<sup>42</sup>

The obtained SCC-DFTB geometries of the S–O-bonded radicals in peptides suggests that their electronic structure should



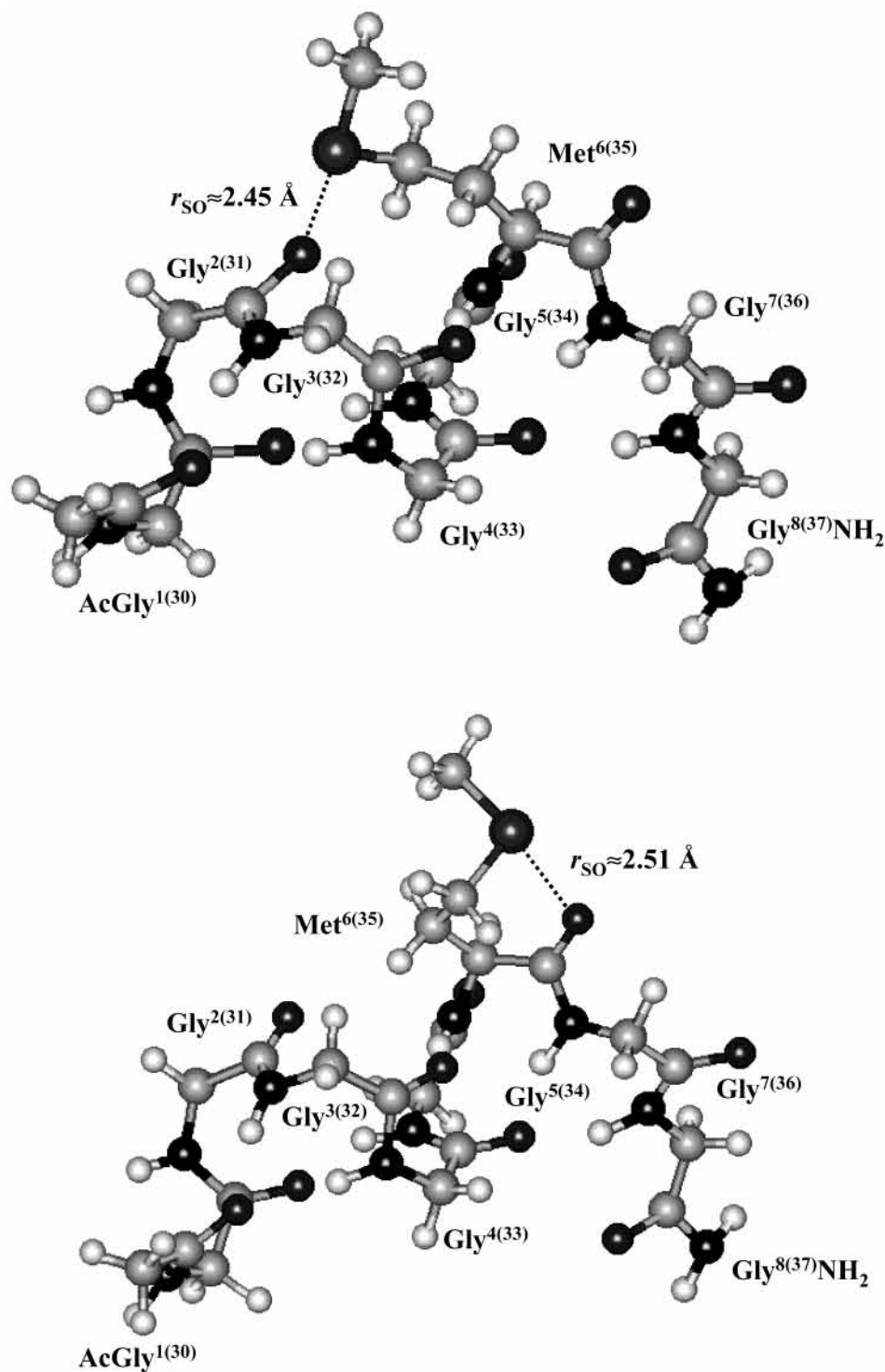


**Figure 4.** The SCC-DFTB calculated geometries of radicals  $2i_{(1,16)}^{*+}$  (upper panel) and  $2i_{(1,6)}^{*+}$  (lower panel).

not be substantially different from that observed for small molecules, which are quite completely described by experimental and higher level computational techniques. However, more detailed physicochemical properties, important for the investigations of the redox-dependent mechanism of  $\beta$ AP toxicity, require theoretical studies that are more detailed. Nevertheless, based on the analogy between the S–O bonds in the peptides and in the model compounds **1c**, **2c**, **2d**, and **2e** we may attempt to estimate the reduction potential of the  $\beta$ AP-(Met<sup>35</sup>) sulfur radical cation, stabilized through S–O bond formation: we believe that the peak reduction potential of the thioether sulfur involved in the interaction with the oxygen atom of the amide functionality should not be substantially different

from that observed experimentally for compound **1c** (0.85 V (vs Ag/AgNO<sub>3</sub>)).<sup>19</sup>

### Conclusions

Hybrid density functional (B3LYP) calculations give important information on the structures and properties of S–O three-electron-bonded radicals. Their calculated physicochemical properties show a reasonable agreement with experimental results.

The novel SCC-DFTB method is able to reliably reproduce structures and relative energies of various three-electron-bonded radicals previously computed by DFT methods. Instead, AM1

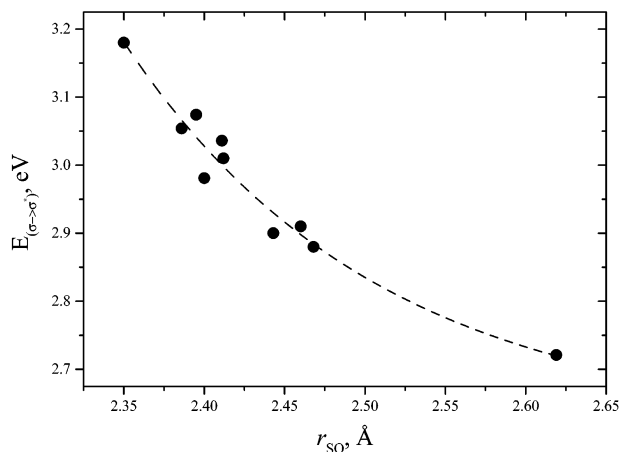


**Figure 5.** Variation of the TD-DFT-computed wavelengths of  $\lambda_{\max}$  with the DFT-optimized S...O bond length.

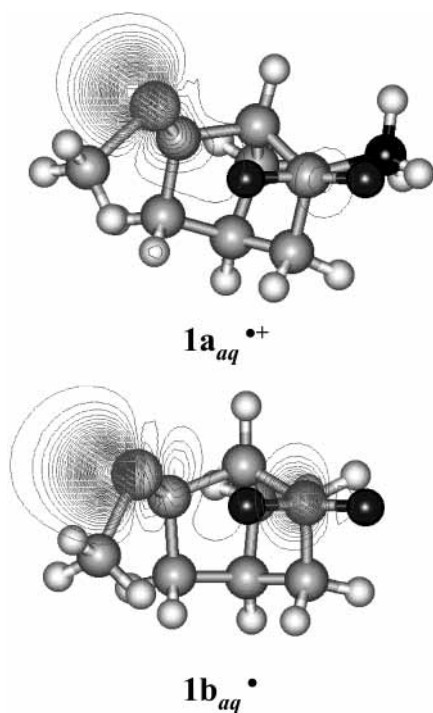


**Figure 6.** Two-dimensional (2D) contour plot of the DFT-IEFPCM calculated total spin density in radicals  $1a_{aq}^+$  and  $1b_{aq}^{\bullet}$ .

and PM3 methods show substantial deficiencies in describing important structural parameters such as the lengths of the three-electron bonds. The discrepancies between the SCC-DFTB method and the DFT (B3LYP) method for medium-sized basis sets (6-311+G(d)) also show the need for higher level calculations, since systematic errors found for small molecules may add up when investigating longer polypeptides. Compared to the deviation between the ab initio methods, the overall performance of the SCC-DFTB method seems to be satisfying. The method is promising and gives a reliable alternative to aforementioned methods, especially for large-scale biomolecular systems. However, the importance of solvent effects on chemical properties and reactivity of the S—O-bonded species could hardly be overestimated; thus the interaction between the system and the surrounding medium must be taken into account to achieve its realistic physicochemical description. For example, the peak reduction potential of the  $\beta$ AP(Met<sup>35</sup>) sulfur radical cation, stabilized through S—O bond formation, would be quite precisely estimated with low computational cost if implicit water solvation effects were included into the SCC-DFTB code.

**Acknowledgment.** Part of this work was achieved in a research group participating in The Research Training Network (Sulfur Radical Chemistry of Biological Significance: The Protective and Damaging Roles of Thiol and Thioether Radicals" (SULFRAD) of the European Commission). Part of this work was supported by NIH 2P01AG12993. Part of the computations were performed employing the computing resources of the Interdisciplinary Center for Mathematical and Computation Modeling at the University of Warsaw, Poland (ICM G24-13).

**Supporting Information Available:** Cartesian coordinates (in Å) for structures as well as total energies of the calculated radicals. This material is available free of charge via the Internet at <http://pubs.acs.org>.

## References and Notes

- Burling, F. T.; Goldstein, B. M. *J. Am. Chem. Soc.* **1992**, *114*, 2313.
- Nagao, Y.; Hirata, T.; Goto, S.; Sano, S.; Kakehi, A.; Iizuka, K.; Shiro, M. *J. Am. Chem. Soc.* **1998**, *120*, 3104.
- Wu, S.; Greer, A. *J. Org. Chem.* **2000**, *65*, 4883.
- Reznik, R.; Greer, A. *Chem. Res. Toxicol.* **2000**, *13*, 1193.
- Brandt, W.; Golbraikh, A.; Tager, M.; Lendeckel, U. *Eur. J. Biochem.* **1999**, *261*, 89.
- Taylor, J. C.; Markham, G. D. *J. Biol. Chem.* **1999**, *274*, 32909.
- Iwaoka, M.; Takemoto, S.; Okada, M.; Tomoda, S. *Chem. Lett.* **2001**, *73*, 1611.
- Iwaoka, M.; Takemoto, S.; Okada, M.; Tomoda, S. *Bull. Chem. Soc. Jpn.* **2002**, *75*, 1611.
- Vogt, W. *Free Radical Biol. Med.* **1995**, *18*, 93.
- Pryor, W. A.; Jin, X.; Squadrito, G. L. *Proc. Natl. Acad. Sci. U.S.A.* **1994**, *91*, 11173.
- Pryor, W. A.; Squadrito, G. L. *Am. J. Physiol.* **1995**, *268*, L699.
- Moreno, J.; Pryor, W. A. *Chem. Res. Toxicol.* **1992**, *5*, 425.
- Hühner, A. F. R.; Gerber, N. C.; Ortiz de Montelano, P. R.; Schöneich, C. *Chem. Res. Toxicol.* **1996**, *9*, 484.
- Perkins, C. W.; Martin, J. C.; Arduengo, A. J.; Lau, W.; Alegria, A.; Kochi, J. K. *J. Am. Chem. Soc.* **1980**, *102*, 7753.
- Glass, R. S.; Hojjatie, M.; Wilson, G. S.; Mahling, S.; Göbl, M.; Asmus, K.-D. *J. Am. Chem. Soc.* **1984**, *106*, 5382.
- Asmus, K.-D.; Göbl, M.; Hiller, K.-O.; Mahling, S.; Mönig, J. *J. Chem. Soc., Perkin Trans. 2* **1985**, 641.
- Chatgililoglu, C.; Castelhana, A. L.; Griller, D. *J. Org. Chem.* **1985**, *50*, 2516.
- Mahling, S.; Asmus, K.-D.; Glass, R. S.; Hojjatie, M.; Wilson, G. S. *J. Org. Chem.* **1987**, *52*, 3717.
- Glass, R. S.; Petsom, A.; Hojjatie, M.; Coleman, B. R.; Duchek, J. R.; Klug, J.; Wilson, G. S. *J. Am. Chem. Soc.* **1988**, *110*, 4772.
- Bobrowski, K.; Holcman, J. *J. Phys. Chem.* **1989**, *93*, 6381.
- Mohan, H. *J. Chem. Soc., Perkin Trans. 2* **1990**, 1821.
- Chatgililoglu, C. In *The Chemistry of Sulphenic Acids and Their Derivatives*; Patai, S., Ed.; John Wiley & Sons Ltd.: New York, 1990; pp 549–569.
- Steffen, L. K.; Glass, R. S.; Sabahi, M.; Wilson, G. S.; Schöneich, C.; Mahling, S.; Asmus, K.-D. *J. Am. Chem. Soc.* **1991**, *113*, 2141.
- Mohan, H.; Mittal, J. P. *J. Chem. Soc., Perkin Trans. 2* **1992**, 207.
- Schöneich, C.; Bobrowski, K. *J. Am. Chem. Soc.* **1993**, *115*, 6538.
- Bobrowski, K.; Schöneich, C. *J. Chem. Soc., Chem. Commun.* **1993**, 795.
- Marciniak, B.; Bobrowski, K.; Hug, G. L.; Rozwadowski, J. *J. Phys. Chem.* **1994**, *98*, 4854.
- Pogocki, D. Ph.D. Thesis, Study on the hydroxyl radical induced reactions in amino acids and peptides containing thioether group; Institute of Nuclear Chemistry and Technology, Warsaw, Poland, 1996.
- Bobrowski, K.; Hug, G. L.; Marciniak, B.; Miller, B. L.; Schöneich, C. *J. Am. Chem. Soc.* **1997**, *119*, 8000.
- Bobrowski, K.; Pogocki, D.; Schöneich, C. *J. Phys. Chem. A* **1998**, *102*, 10512.
- Glass, R. S.; Hojjatie, M.; Petsom, A.; Wilson, G. S.; Göbl, M.; Mahling, S.; Asmus, K.-D. *Phosphorus Sulfur Relat. Elem.* **1985**, *23*, 143.
- Glass, R. S.; Duchek, J. R.; Klug, J.; Wilson, D. *J. Am. Chem. Soc.* **1977**, *99*, 7349.
- Glass, R. S. *Xenobiotica* **1995**, *25*, 637.
- Levine, R. L.; Mosoni, L.; Berlett, B. S.; Stadtman, E. R. *Proc. Natl. Acad. Sci. U.S.A.* **1996**, *93*, 15036.
- Chao, C. C.; Ma, Y. S.; Stadtman, E. R. *Proc. Natl. Acad. Sci. U.S.A.* **1997**, *94*, 2969.
- Moskovitz, J.; Berlett, B. S.; Poston, J. M.; Stadtman, E. R. *Proc. Natl. Acad. Sci. U.S.A.* **1997**, *94*, 9585.

- (37) Moskovitz, J.; Flescher, E.; Berlett, B. S.; Azare, J.; Poston, J. M.; Stadtman, E. R. *Proc. Natl. Acad. Sci. U.S.A.* **1998**, *95*, 14071.
- (38) Butterfield, A. D. *Chem. Res. Toxicol.* **1997**, *10*, 495.
- (39) Sayre, L. M.; Zagorski, M. G.; Surewicz, W. K.; Krafft, G. A.; Perry, G. *Chem. Res. Toxicol.* **1997**, *10*, 518.
- (40) Coles, M.; Bicknell, W.; Watson, A. A.; Fairlie, D. P.; Craik, D. J. *Biochemistry* **1998**, *37*, 11064.
- (41) Bondi, A. J. *J. Phys. Chem.* **1964**, *68*, 441.
- (42) Pogocki, D.; Schöneich, C. *Chem. Res. Toxicol.* **2002**, *15*, 408.
- (43) Kanski, J.; Aksenova, M.; Schöneich, C.; Butterfield, D. A. *Free Radic. Biol. Med.* **2002**, *32*, 1205.
- (44) Schöneich, C.; Pogocki, D.; Wisniowski, P.; Hug, G.; Bobrowski, K. *J. Am. Chem. Soc.* **2000**, *122*, 10224.
- (45) Schöneich, C.; Pogocki, D.; Hug, G.; Bobrowski, K. Unpublished results.
- (46) Dewar, M. S. J.; Zoebish, E. G.; Healy, E. F.; Stewart, J. J. P. *J. Am. Chem. Soc.* **1977**, *99*, 1685.
- (47) Dewar, M. S. J.; Yuan, Y.-C. *Inorg. Chem.* **1990**, *29*, 3881.
- (48) Stewart, J. J. P. *J. Comput. Chem.* **1991**, *10*, 221.
- (49) Stewart, J. J. P. *J. Comput. Chem.* **1989**, *10*, 209.
- (50) Clark, T. In *Sulfur-Centered Reactive Intermediates in Chemistry and Biology*; Chatgililoglu, C., Asmus, K.-D., Eds.; Plenum Press: New York, 1990; pp 1–6.
- (51) Niehaus, T. A.; Elstner, M.; Frauenheim, T.; Suhai, S. *J. Mol. Struct. (THEOCHEM)* **2001**, *541*, 185.
- (52) Cui, Q.; Elstner, M.; Kaxiras, E.; Frauenheim, T.; Karplus, M. *J. Phys. Chem. B* **2001**, *105*, 569.
- (53) Cui, Q.; Elstner, M.; Karplus, M. *J. Phys. Chem. B* **2002**, *106*, 2721.
- (54) Elstner, M.; Frauenheim, T.; Kaxiras, E.; Seifert, G.; Suhai, S. *Phys. Status Solidi B* **2000**, *217*, 357.
- (55) Elstner, M.; Jalkanen, K. J.; Knapp-Mohammaday, M.; Frauenheim, T.; Suhai, S. *Chem. Phys.* **2000**, *256*, 15.
- (56) Elstner, M.; Porezag, D.; Jungnickel, G.; Elsner, J.; Haugk, M.; Frauenheim, T.; Suhai, S.; Seifert, G. *Phys. Rev. B* **1998**, *58*, 7260.
- (57) Frauenheim, T.; Seifert, G.; Elstner, M.; Hajnal, Z.; Jungnickel, G.; Porezag, D.; Suhai, S.; Scholz, R. *Phys. Status Solidi B* **2000**, *217*, 41.
- (58) Han, W.-G.; Elstner, M.; Jalkanen, K. J.; Frauenheim, T.; Suhai, S. *Int. J. Quantum Chem.* **2000**, *78*, 459.
- (59) Liu, H.; Elstner, M.; Kaxiras, E.; Frauenheim, T.; Hermans, J.; Yang, W. *Proteins* **2001**, *44*, 484.
- (60) Frauenheim, T.; Seifert, G.; Elstner, M.; Niehaus, T. A.; Köhler, C.; Amkreutz, M.; Stenberg, M.; Hajnal, Z.; DiCalo, A.; Suhai, S. *J. Phys. Condens. Matter* **2002**, *14*, 315347.
- (61) Elstner, M.; Jalkanen, K. J.; Knapp-Mohammaday, M.; Frauenheim, T.; Suhai, S. *Chem. Phys.* **2001**, *263*, 203.
- (62) Bohr, H. G.; Jalkanen, K. J.; Elstner, M.; Frimand, K.; Suhai, S. *Chem. Phys.* **1999**, *246*, 13.
- (63) Asmus, K.-D. *Acc. Chem. Res.* **1979**, *12*, 436.
- (64) Clark, T. *J. Comput. Chem.* **1981**, *2*, 261.
- (65) Fernandez, P. F.; Ortiz, J. V.; Walters, E. A. *J. Chem. Phys.* **1986**, *84*, 1653.
- (66) Gill, P. M. W.; Radom, L. *J. Am. Chem. Soc.* **1988**, *110*, 4931.
- (67) Clark, T. *J. Am. Chem. Soc.* **1988**, *110*, 1672.
- (68) Carmichael, I. *Acta Chem. Scand.* **1997**, *51*, 567.
- (69) Bickelhaupt, F. M.; Diefenbach, A.; de Visser, S. P.; de Konning, L. J.; Nibbering, N. M. I. *J. Phys. Chem. A* **1998**, *102*, 9533.
- (70) Carmichael, I. *Nukleonika* **2000**, *41*, 11.
- (71) Rauk, A.; Armstrong, D. A.; Fairlie, D. P. *J. Am. Chem. Soc.* **2000**, *122*, 9761.
- (72) Braida, B.; Hazebrucq, S.; Hiberty, P. C. *J. Am. Chem. Soc.* **2002**, *124*, 2371.
- (73) Pogocki, D.; Schöneich, C. *J. Org. Chem.* **2002**, *67*, 1526.
- (74) Maity, D. K. *J. Am. Chem. Soc.* **2002**, *124*, 8321.
- (75) Becke, A. D. *J. Chem. Phys.* **1993**, *98*, 5648.
- (76) Bauschlicher, C. W., Jr.; Partridge, H. *Chem. Phys. Lett.* **1995**, *240*, 533.
- (77) Zwier, J. M.; Wichers Hoeth, J.; Brouwer, A. M. *J. Org. Chem.* **2001**, *66*, 466.
- (78) Carmichael, I. *J. Phys. Chem. A* **1997**, *101*, 4633.
- (79) Hug, G. L.; Carmichael, I.; Fessenden, R. W. *J. Chem. Soc., Perkin Trans. 2* **2000**, 907.
- (80) Eriksson, L. A.; Malkina, O. L.; Malkin, V.; Salahub, D. R. *J. Chem. Phys.* **1994**, *100*, 5066.
- (81) Barone, V.; Adamo, C.; Russo, N. *Int. J. Quantum Chem.* **1994**, *52*, 963.
- (82) O'Malley, P. J. *J. Phys. Chem. A* **1997**, *101*, 6334.
- (83) O'Malley, P. J. *J. Comput. Chem.* **1999**, *20*, 1292.
- (84) Davidson, E. R.; Feller, D. *Chem. Rev.* **1986**, *86*, 681.
- (85) Labanowski, J. K. *Simplified introduction to ab initio basis sets. Terms and notation.* www.chem.utas.edu.au/staff/yatesb/modules/mod5/jan\_basis.html, Ohio Supercomputer Center, Columbus, OH, 2001; pp 1–13.
- (86) Jensen, F. *Introduction to Computational Chemistry*; John Wiley & Sons Ltd.: Chichester, UK, 1999; pp 1–429.
- (87) Cancès, E.; Mennucci, B.; Tomasi, J. *J. Chem. Phys.* **1997**, *107*, 3032.
- (88) Casida, M. E.; Jamorski, C.; Casida, C.; Salahub, D. R. *J. Chem. Phys.* **1998**, *108*, 4439.
- (89) *HyperChem Computational Chemistry*. Hypercube Inc.: Waterloo, Ontario, Canada, 1994; pp 189–249.
- (90) Ridley, J. E.; Zerner, M. C. *Theor. Chim. Acta* **1976**, *42*, 223.
- (91) Bacon, A. D.; Zerner, M. C. *Theor. Chim. Acta* **1979**, *53*, 21.
- (92) Ridley, J. E.; Zerner, M. C. *J. Mol. Spectrosc.* **1979**, *76*, 71.
- (93) Zerner, M. C. In *Reviews of Computational Chemistry*; VCH: New York, 1991; pp 313–366.
- (94) Clark, T. In *Recent Experimental and Computational Advances in Molecular Spectroscopy*; Fausto, R., Ed.; Kluwer Academic: Dordrecht-Boston, 1993; pp 369–380.
- (95) Brooks, B. R.; Bruccoleri, R. E.; Olafson, B. D.; States, D. J.; Swaminathan, S.; Karplus, M. *J. Comput. Chem.* **1983**, *4*, 187.
- (96) Karelson, M. M.; Zerner, M. C. *J. Phys. Chem.* **1992**, *96*, 6947.
- (97) Jorgensen, W. L.; Chandraskhar, J.; Madura, J.; Impey, R. W.; Klein, M. L. *J. Phys. Chem.* **1983**, *79*, 926.
- (98) Reiher, W. E. Ph.D. Dissertation, Harvard University, Cambridge MA, 1985.
- (99) *HyperChem Computational Chemistry*; Hypercube Inc.: Waterloo, Ontario, Canada, 1994; pp 139–185.
- (100) Frisch, M. J.; Trucks, G. W.; Schlegel, H. B.; Scuseria, G. E.; Robb, M. A.; Cheeseman, J. R.; Zakrzewski, V. G.; Montgomery, J. A., Jr.; Stratmann, R. E.; Burant, J. C.; Dapprich, S.; Millam, J. M.; Daniels, A. D.; Kudin, K. N.; Strain, M. C.; Farkas, O.; Tomasi, J.; Barone, V.; Cossi, M.; Cammi, R.; Mennucci, B.; Pomelli, C.; Adamo, C.; Clifford, S.; Ochterski, J.; Petersson, G. A.; Ayala, P. Y.; Cui, Q.; Morokuma, K.; Malick, D. K.; Rabuck, A. D.; Raghavachari, K.; Cioslowski, J.; Ortiz, J. V.; Baboul, A. G.; Stefanov, B. B.; Liu, G.; Liashenko, A.; Piskorz, P.; Komaromi, I.; Gomperts, R.; Martin, R. L.; Fox, D. J.; Keith, T.; Al-Laham, M. A.; Peng, C. Y.; Nanayakkara, A.; Gonzalez, C.; Challacombe, M.; Gill, P. M. W.; Johnson, B.; Chen, W.; Wong, M. W.; Andres, J. L.; Head-Gordon, M.; Replogle, E. S.; Pople, J. A. *Gaussian 98*, Revision A.7; Gaussian Inc.: Pittsburgh, PA, 1998.
- (101) *HyperChem Computational Chemistry*; Hypercube Inc.: Waterloo, Ontario, Canada, 1996.
- (102) ISIS Draw 2.2.4. <http://www.mdli.com>, MDL Information Systems Inc. 2001.
- (103) Leach, A. R. *Molecular modelling: principles and applications*; Longman: Harlow, England, 1996.
- (104) Laaksonen, L. gOpenMol 2.10. <http://laaksonen.csc.fi/gopenmol/gopenmol.html>, 2001.
- (105) Walters, P.; Stahl, M. Babel 1.6. <http://www.chem.ohiou.edu/~dolata/babel.html>, 1999.
- (106) Rauk, A. *Orbital Interaction Theory of Organic Chemistry*; John Wiley & Sons: New York, 2001; pp 1–343.
- (107) Krygowski, T. M.; Kalinowski, M. K.; Turowska-Tryk, I.; Hiberty, P. C.; Milart, P.; Silvestro, A.; Topsom, R. D.; Daehne, S. *Struct. Chem.* **1991**, *2*, 71.
- (108) Sülzle, D.; Drewello, T.; Scharz, H. In *Sulfur-Centered Reactive Intermediates in Chemistry and Biology*; Chatgililoglu, C., Asmus, K.-D., Eds.; Plenum Press: New York, 1990; pp 185–192.
- (109) Wilson, D. In *Sulfur-Centered Reactive Intermediates in Chemistry and Biology*; Chatgililoglu, C., Asmus, K.-D., Eds.; Plenum Press: New York, 1990; pp 83–92.
- (110) Armstrong, D. A. In *S-centered radicals*; Alfassi, Z.B., Ed.; John Wiley & Sons: New York, 1999; pp 27–61.
- (111) Dill, K. A.; Bromberg, S.; Yue, K.; Fiebig, K. M.; Yee, D. P.; Thomas, P. D.; Chan, H. S. *Protein Sci.* **1995**, *4*, 561.
- (112) Perrin, C. L.; Nielson, J. B. *Annu. Rev. Phys. Chem.* **1997**, *48*, 511.
- (113) Dziembowska, T. *Polish J. Chem.* **1994**, *68*, 1455.
- (114) Wu, J.; Gard, E.; Bregar, J.; Green, M. K.; Lebrilla, C. *J. Am. Chem. Soc.* **1995**, *117*, 9900.
- (115) Deng, Y.; Illies, A. J.; James, M. A.; McKee, M. L.; Peschke, M. *J. Am. Chem. Soc.* **1995**, *117*, 420.
- (116) Clark, T. In *Sulfur-Centered Reactive Intermediates in Chemistry and Biology*; Chatgililoglu, C., Asmus, K.-D., Eds.; Plenum Press: New York, 1990; pp 13–18.
- (117) McKee, M. L. *J. Phys. Chem.* **1993**, *97*, 10971.
- (118) Bobrowski, K.; Pogocki, D.; Schöneich, C.; Hug, G. L.; Marciniak, B. Unpublished results.
- (119) Ooi, T.; Obatake, M.; Nemethy, G.; Scheraga, H. A. *Proc. Natl. Acad. Sci. U.S.A.* **1987**, *84*, 3086.
- (120) Moriguchi, I.; Hirono, S.; Liu, Q.; Nakagome, I.; Matsushita, Y. *Chem. Pharm. Bull. (Tokyo)* **1992**, *40*, 127.
- (121) Moriguchi, I.; Hirono, S.; Nakagome, I.; Hirano, H. *Chem. Pharm. Bull. (Tokyo)* **1994**, *42*, 976.